Bioactive Materials 32 (2024) 304–318

Contents lists available at ScienceDirect

Bioactive Materials

journal homepage: www.keaipublishing.com/en/journals/bioactive-materials

Dual-response of multi-functional microsphere system to ultrasound and microenvironment for enhanced bone defect treatment

Qingxu Song [a,b], Dianwei Wang [b], Haoyu Li [a,b], Zongliang Wang [b], Songjia Sun [c], Zhenyu Wang [a], Yi Liu [a], Sien Lin [d], Gang Li [d], Shaokun Zhang [a,**], Peibiao Zhang [b,*]

[a] Department of Spine Surgery, The First Hospital of Jilin University, Changchun, 130021, China
[b] Key Laboratory of Polymer Ecomaterials, Changchun Institute of Applied Chemistry, Chinese Academy of Sciences, Changchun, 130022, China
[c] Department of Dermatology, Second Hospital of Jilin University, Changchun, 130022, China
[d] Department of Orthopaedics and Traumatology and Li Ka Shing Institute of Health Sciences, Prince of Wales Hospital, The Chinese University of Hong Kong, Shatin, Hong Kong Special Administrative Region of China

ARTICLE INFO

Keywords:
BMP-2
Multi-functional microsphere
Bone defect repair
Bone injury microenvironment
Immune microenvironment

ABSTRACT

Using bone tissue engineering strategies to achieve bone defect repair is a promising modality. However, the repair process outcomes are often unsatisfactory. Here we properly designed a multi-functional microsphere system, which could deliver bioactive proteins under the dual response of ultrasound and microenvironment, release microenvironment-responsive products on demand, reverse bone injury microenvironment, regulate the immune microenvironment, and achieve excellent bone defect treatment outcomes. In particular, the MnO_2 introduced into the poly(lactic-co-glycolic acid) (PLGA) microspheres during synthesis could consume the acid produced by the degradation of PLGA to protect bone morphogenetic protein-2 (BMP-2). More importantly, MnO_2 could consume reactive oxygen species (ROS) and produce Mn^{2+} and oxygen (O_2), further promoting the repair of bone defects while reversing the microenvironment. Moreover, the reversal of the bone injury microenvironment and the depletion of ROS promoted the polarization of M1 macrophages to M2 macrophages, and the immune microenvironment was regulated. Notably, the ultrasound (US) irradiation used during treatment also allowed the on-demand release of microenvironment-responsive products. The multi-functional microsphere system combines the effects of on-demand delivery, reversal of bone injury microenvironment, and regulation of the immune microenvironment, providing new horizons for the clinical application of protein delivery and bone defect repair.

1. Introduction

Trauma, orthopedic surgery, infection, and bone tumor resection can cause bone defects. However, achieving ideal bone defect repair and treating its associated diseases are still challenging [1–4]. Bone tissue engineering was born and has become a research hotspot after decades of development [5–9], which emphasizes the inoculation of cells on scaffolds or loading of growth factors to achieve slow release while mimicking the tissue regeneration microenvironment *in vivo* to accelerate the quality and rate of tissue regeneration [10–12]. Among them, growth factor-based therapy is considered the most effective strategy to guide tissue regeneration. Bone morphogenetic protein-2 (BMP-2), which significantly increases alkaline phosphatase activity, has been widely used in treating bone defects [13,14]. However, supra-physiological doses of BMP-2 can lead to many side effects, such as excessive inflammatory responses and ectopic bone formation [15,16].

In addition, the treatment of bone defect repair is a comprehensive process of defect-regeneration and inflammation-repair [17]. Promoting osteoblast regeneration with BMP-2 alone is sometimes difficult to achieve the desired repair effect. One reason is that the bone injury microenvironment is formed at the bone injury site characterized by inflammation, acidity, lack of oxygen, and high expression of reactive oxygen species (ROS) [18,19]. If the microenvironment is not reversed, the new bone formation would be difficult [20].

Peer review under responsibility of KeAi Communications Co., Ltd.
* Corresponding author.
** Corresponding author.
E-mail addresses: shaokun@jlu.edu.cn (S. Zhang), zhangpb@ciac.ac.cn (P. Zhang).

https://doi.org/10.1016/j.bioactmat.2023.10.007
Received 21 July 2023; Received in revised form 21 September 2023; Accepted 7 October 2023

On the other hand, heterogeneous macrophages play a key role in the bone injury process [17]. During acute injury, M1-type (pro-inflammatory) macrophages release inflammatory mediators, build a pro-inflammatory microenvironment, and promote angiogenesis [21,22]. However, if M1 macrophages do not convert to M2 macrophages in time, it will affect bone injury repair [23]. The persistence of inflammation in the bone injury microenvironment will affect the conversion of M1 to M2 [24]. The most serious impact is on ROS, which can promote M1 polarization through the nuclear factor kappa light chain enhancer of activated B cells (NF-κB) pathway [25]. Therefore, the bone injury microenvironment equally affects the immune microenvironment.

Therefore, the limitations of delivery, bone injury microenvironment, and immune microenvironment should be addressed simultaneously when BMP-2 is used for bone defect repair to achieve optimal therapeutic outcomes. Biodegradable poly(lactic-co-glycolic acid) (PLGA) microspheres with excellent biocompatibility have been widely used for the slow release of peptides and proteins [26]. However, the acidic degradation products of PLGA (lactic and glycolic acids) accumulate in the implant, creating an acidic internal environment [27,28]. Using PLGA microspheres to carry BMP-2 will undoubtedly lead to structural instability, decomposition, and even inactivation of BMP-2. In addition, the conventional strategy of using PLGA to deliver protein drugs generally shows that it is difficult to release the drugs on demand, and the therapeutic effect is poor. Therefore, both the internal acidic environment and the difficulty of on-demand release should be addressed when delivering BMP-2 by PLGA. Applying low-frequency ultrasound (US) for spatiotemporally controlled drug release has been widely reported [29], and the US is widely used in clinical practice for its biosafety and, more valuable, its facilitative effect on bone defect repair. Therefore, using US irradiation for the on-demand controlled release of BMP-2 from PLGA to treat bone defects is an appropriate option.

A buffering agent can be incorporated into the microspheres to overcome the acidic environment within the microspheres [28]. MnO_2 has been intensively explored in tumor therapy and bone defect repair in recent years [19]. MnO_2 reacts with acid and hydrogen peroxide to produce Mn^{2+} and oxygen (O_2) [30]. If MnO_2 is introduced into PLGA, it can neutralize the internal acidic environment, protect BMP-2, deplete the ROS and acid in the bone injury microenvironment, and solve the problem of a lack of O_2. Furthermore, the generated Mn^{2+} plays a key role in muscle and bone metabolism by accelerating fracture healing and enhancing osteogenesis [31]. In this way, the introduction of MnO_2 addresses the acidity within PLGA and reverses the bone injury microenvironment. More importantly, due to the depletion of ROS and reversal of the microenvironment, it can promote the polarization of M1 to M2 macrophages, reduce inflammation, regulate the immune microenvironment, and increase the osteogenic effect. Therefore, careful designing of MnO_2 introduction while delivering BMP-2 by PLGA and releasing it on demand under the action of the US can solve the problems of delivery, bone injury microenvironment, and immune microenvironment simultaneously to enhance the therapeutic effects on the bone defect.

In this work, we prepared a multi-functional microsphere system for US application and microenvironmental dual-responsive protein delivery to achieve on-demand release of microenvironmental responsive products, reverse bone injury microenvironment, and modulate immune microenvironment for bone defect treatment in tandem with multiple functions. Hollow MnO_2 (H–MnO_2) nanoparticles were first synthesized to increase the contact area between MnO_2 and the medium and effectively loaded with BMP-2 after cationization. The microsphere system was prepared by a modified solid-in-oil-in-water (S/O/W) emulsion technique with PLGA [32]. The introduction of MnO_2 neutralized the acid generated from PLGA degradation and bone injury microenvironment, protected the structure of BMP-2, and promoted the proliferation of osteoblasts. Moreover, MnO_2 could consume H_2O_2 produced in the bone injury microenvironment with the participation of acid and produced Mn^{2+} and O_2, further promoting the repair of bone defects while reversing the microenvironment. Furthermore, the reversal of the bone injury microenvironment and the consumption of ROS promoted the polarization of M1 macrophages to M2 macrophages, regulated the immune microenvironment, and increased the osteogenic effect. In addition, we used US irradiation during treatment, which allowed the on-demand release of microenvironment-responsive products. This multi-functional microsphere system promoted cell growth and osteogenic differentiation at the cellular level, resulting in excellent bone defect repair at the animal level under the combined effects of multiple functions. In addition, the components of the multi-functional microsphere system are biodegradable and have good biological safety, which provides a good foundation for clinical application.

2. Material and methods

2.1. Materials

PLGA (LA/GA = 80:20, Mw = 100 kDa) was obtained from Changchun Institute of Applied Chemistry, Chinese Academy of Sciences. Poly (allylamine hydrochloride) (PAH) was purchased from Shanghai Macklin Biochemical Technology Co., Ltd (Shanghai, China). BMP-2 was bought from Sino Biological, Inc. (Beijing, China). Mouse embryonic osteoblast precursor cells (MC3T3-E1) were obtained from the Shanghai Institute of Biochemistry and Cell Biology. Calcein-AM/propidium iodide (Calcein-AM/PI) and LysoSensor™ Yellow/Blue were purchased from Thermo Fisher Scientific, Inc. (Waltham, MA). Alkaline phosphatase (ALP) staining kit, alizarin red staining (ARS) staining kit, cell counting kit-8 (CCK-8), and ROS assay kit (DCFH-DA) were bought from Beyotime Biotechnology (Shanghai, China). The liver function and kidney function assay kits were purchased from Nanjing Jiancheng Bioengineering Institute (Jiangsu, China). All the other reagents were obtained from Sinopharm Chemical Reagent Co. Ltd. (China).

2.2. Instruments

The size of nanoparticles was determined by transmission electron microscope (TEM) (JEM-1011, JEOL, Tokyo, Japan) and particle size analyzer (ZEN3600, Zetasizer Ultra, MALVERN PANALYTICAL LIMITED, U.K.). The surface morphology and elemental distribution of microspheres were measured by the field emission scanning electron microscope (Zeiss Merlin FE-SEM) with an EDS detector. The X-ray diffraction (XRD) analysis of nanoparticles was evaluated by the X-ray diffractometer (D8 ADVANCE, Bruker, Germany). The VG ESCALAB MKII spectrometer (UK) was used to record the X-ray photoelectron spectroscopy (XPS) to analyze the elemental composition and chemical states. The N_2 isotherm was evaluated by the volumetric analyzer (Autosorb iQ, Quantachrome, USA). The content of the Mn element of microspheres was assessed by inductively coupled plasma-mass spectrometry (ICP-MS) (Thermo Fisher Scientific, USA). DJO-2776 ultrasound meter was used for the US source.

2.3. The preparation of H–MnO_2 nanoparticles

The SiO_2 nanoparticles (SiO_2 NPs) were synthesized according to the reported method [33]. The absolute ethanol (16.25 mL), aqueous ammonia (9 mL), and deionized water (24.75 mL) were added to a round bottom flask and stirred at 50 ^{O}C for 5 min (1100 rpm). After that, a homogeneous mixture of tetraethylorthosilicate (TEOS) mixed with absolute ethanol was added into the flask and stirred at 360 rpm for 2 h. The SiO_2 NPs were collected by centrifugation after finishing the reaction (14800 rpm, 5 min).

The obtained SiO_2 NPs (80 mg) were dispersed in deionized water (10 mL), and the potassium permanganate ($KMnO_4$) aqueous solution (30 mg mL^{-1}, 20 mL) was slowly added under ultrasonic conditions, and the ultrasonic was continued for 1 h, and then stirred overnight. After

the reaction, the mixture was centrifuged for 5 min (14800 rpm) and washed 3 times with deionized water to collect SiO_2@MnO_2 nanoparticles(SiO_2@MnO_2 NPs).The obtained SiO_2@MnO_2 NPs were dispersed in sodium carbonate (Na_2CO_3) aqueous solution (2 M, 20 mL) and stirred at 60 ^{O}C overnight. After the reaction, the mixture was centrifuged for 5 min (14800 rpm) and washed 3 times with deionized water to collect H–MnO_2 nanoparticles.

2.4. The preparation of H–MnO_2@PAH@BMP-2 (MPB)

First, H–MnO_2 (5 mg) was dispersed in deionized water (1 mL) and mixed with PAH solution (20 mg mL^{-1}, 1 mL). After stirring for 2 h, H–MnO_2@PAH (MPAH) was obtained by centrifugation for 5 min (14800 rpm) and washing 3 times with deionized water [34]. After that, BMP-2 loading was carried out, and MPAH solution (5 mg mL^{-1}) was mixed with BMP-2 (10 μg mL^{-1}) for 12 h to obtain MPB.

2.5. The preparation of H–MnO_2@PAH@BMP-2@PLGA (MPBP) microspheres

The microsphere system was prepared by a modified S/O/W emulsion technique [32]. In brief, a 25% w/v PLGA/DCM solution was formed by dissolving PLGA (500 mg) in dichloromethane (DCM) (2 mL). Afterward, the prepared MPB was added into the above solution for thorough mixing, and dispersed in 2% PVA (25 ml) solution by a homogenizer (IKA, Germany) (5000 rpm). Then the mixture was dropped into a 1% PVA (50 mL, Mw = 67000) aqueous solution and stirred overnight at room temperature. The MPBP microspheres were collected using centrifugation and washed several times with deionized water prior to lyophilization. The preparation method of BMP-2@PLGA microspheres: BMP-2 solution was added into the 25% w/v PLGA/DCM solution, after mixing, the mixture was dispersed in 2% PVA solution by a homogenizer. Then the mixture was dropped into a 1% PVA aqueous solution and stirred overnight at room temperature. The pure PLGA microspheres were prepared in a similar manner.

2.6. The ability of oxygen production

In order to assay the oxygen production ability of MPBP microspheres. MPBP was mixed well with H_2O_2 in deoxygenated water. During the incubation period, the oxygen content of the mixture was recorded using a dissolved oxygen meter (Shanghai San-Xin Instrumentation, Inc.).

2.7. Loading rate of MPBP

The loading rate of MPBP on proteins was calculated using the content of MnO_2. Protein content in MPB was measured using the bicinchoninic acid (BCA) kit. The Mn element was quantitatively analyzed by ICP-MS, and the content of MnO_2 was calculated by applying the following equation:

$$\text{DLC (wt \%)} = (\text{weight of loaded } MnO_2/\text{total weight of MPBP}) \times 100\%$$

2.8. Release of BMP-2 and Mn ions

In order to test the release under different conditions, six groups were set up in the test experiment: PBS (pH = 7.4), PBS (pH = 7.4) + H_2O_2, PBS (pH = 7.4) + H_2O_2/US, PBS (pH = 5.5), PBS (pH = 5.5) + H_2O_2, and PBS (pH = 5.5) + H_2O_2/US (H_2O_2 = 100 μM). In all test groups, the weight of MPBP was 10 mg and the volume of the solution was 5 mL. The mixed solution was placed in a constant temperature shaker at 37 ^{O}C for incubation. 1 mL of supernatant was collected every two days and a new degradation solution was added, where ultrasound interventions (1 MHz, 1 W/cm^2, 3 min) were performed on days 10, 20, and 29 in the ultrasound group. Finally, the concentration of BMP-2 was measured by BCA kit and the concentration of Mn ions was measured by ICP-MS.

2.9. Analysis of pH variation in microspheres

An acidic pH-sensitive probe, LysoSensor Yellow/Blue Dextran (10 kD), was encapsulated in PLGA microspheres and H–MnO_2@PLGA microspheres, imaged by laser confocal microscopy (Nikon, Japan) on days 1, 7, 14, 21, and 28 to evaluate the internal pH changes of the microspheres (Ex: 364 nm and Em: 450 nm and 520 nm).

2.10. Structural integrity analysis of BMP-2

To demonstrate that the introduction of MnO_2 had a protective effect on BMP-2, test experiments were performed. The acidic environment was simulated inside the microspheres, three groups were set up in the test experiment: PBS (pH = 7.4) + BMP-2 group, PBS (pH = 3) + BMP-2 group, and PBS (pH = 3) + BMP-2 + MnO_2 group. The mixed solution was placed in a constant temperature shaker at 37 ^{O}C for incubation. After 3 days, circular dichroism and mass spectrometry were performed separately.

2.11. Cell cytotoxicity

For investigating the *in vitro* cytotoxicity of different groups, in a 24-well plate, MC3T3-E1 cells were seeded at a density of 5×10^4/well and incubated for 24 h. After that, the plate was incubated with various formulations (PBS, MPBP (0.5 %MPB), MPBP (1% MPB), MPBP (2.5% MPB), MPBP (5% MPB), and MPBP (10% MPB)) for 24 h. The viability of MC3T3-E1 cells was assessed using the CCK-8 assay.

2.12. Cell viability and proliferation

In a 24-well plate, MC3T3-E1 cells were seeded at a density of 5×10^4/well and incubated for 24 h. After that, the plate was incubated with various formulations (PBS, PLGA, MnO_2@PLGA, PLGA (100 μM H_2O_2), MnO_2@PLGA (100 μM H_2O_2), PLGA (200 μM H_2O_2), and MnO_2@PLGA (200 μM H_2O_2)), and on days 1, 3, 5, cell proliferation was detected using the CCK-8 assay. On days 1, 3, and 5, live/dead staining was performed with various formulations (PBS, PLGA, MnO_2@PLGA, PBS (100 μM H_2O_2), PLGA (100 μM H_2O_2), and, MnO_2@PLGA (100 μM H_2O_2)).

2.13. Intracellular ROS

In a 24-well plate, MC3T3-E1 cells were seeded at a density of 5×10^4/well and incubated for 24 h. After that, the plate was incubated with various formulations (PBS, PBS (100 μM H_2O_2), PLGA, PLGA (100 μM H_2O_2), MnO_2@PLGA, and MnO_2@PLGA (100 μM H_2O_2)). MC3T3-E1 cells were then incubated with DCFH-DA. An inverted fluorescence microscope (TE2000U, Nikon) was used to perform fluorescence imaging.

2.14. In vitro polarization of RAW 264.7 macrophages

In a 24-well plate, RAW 264.7 cells were seeded at a density of 1×10^5/well. After that, the plate was incubated with various formulations for 24 h. Medium containing lipopolysaccharide (LPS) (500 ng/mL) was added and incubated for 24 h. The cells were fixed in 4% paraformaldehyde (PFA) for 30 min, washed in PBS and incubated in Immunol Staining Blocking Buffer for 1 h. The primary antibody was diluted, 200 μL was added to each well, and incubated overnight at 4 °C. The primary antibody was aspirated and washed with PBS, then 200 μL of the secondary antibody dilution was added to each well and

incubated for 2 h. In addition, the nuclei were stained with DAPI for 2 min. Finally, it was observed by confocal microscopy.

2.15. In vitro osteogenesis

In a 24-well plate, MC3T3-E1 cells were seeded at a density of 5×10^4/well and incubated for 24 h. The test experiments were divided into 7 groups: PBS, US, PLGA, H–MnO_2@PLGA, BMP-2@PLGA, MPBP, and MPBP/US. For MPBP/US group, the US irradiation (1 MHz, 1 W/cm^2, 1 min) was carried out every two days. Staining and quantitative assessments were performed on days 7 and 14 using ALP kit. The mineralized deposition was measured by ARS kit and 10% cetylpyridinium chloride (CPC) on days 14 and 21. A microscope (TE2000U, Nikon) was used for imaging, and a microplate reader (Tecan Infinite M200) was used for absorbance measurement.

2.16. PCR analysis

The expression of osteogenesis and macrophage genes was quantitatively evaluated by reverse transcription-quantitative polymerase chain reaction (RT-qPCR). The primer sequences for each gene were listed in Table S1.

2.17. Rat skull defect model

Sprague-Dawley rats (6–8 weeks) were bought from Vital River Company (Beijing, China). After anesthesia, a surgical trephine was used to create two circular skull bony defects with a diameter of 5 mm in each rat. After implanting different microspheres into the bone defect, the incision was closed, and the rats were lived and fed separately. Rats were euthanized by intraperitoneal injection of pentobarbital on the 7th day, 4th week, and 8th week. All animal studies were carried out according to the guidelines approved by the Animal Welfare and Ethics Committee of Changchun Institute of Applied Chemistry, Chinese Academy of Sciences.

2.18. In vivo bioactive protein protection

PLGA microspheres and MnO_2@PLGA microspheres loaded with LysoSensor Yellow/Blue Dextran were implanted into the skull defects of rats and removed on days 1, 7, and 14 for fluorescence confocal microscopy. PLGA microspheres and MnO_2@PLGA microspheres loaded with enhanced green fluorescent protein (EGFP) were implanted into the skull defects of rats and removed on days 1, 7, and 14 for fluorescence confocal microscopy.

2.19. In vivo osteogenesis

35 rats were randomly assigned to 7 groups: PBS, US, PLGA, H–MnO_2@PLGA, BMP-2@PLGA, MPBP, and MPBP/US. Microspheres were implanted into the bone defect during treatment. For MPBP/US group, the US irradiation (1 MHz, 1 W/cm^2, 3 min) was carried out every week. The body weight of the rats was recorded weekly during the treatment period.

2.20. Microcomputed tomography (Micro-CT) evaluation

Computed tomography analysis was applied using a Micro-CT scanner (PerkinElmer Quantum GX2, USA) to assess microsphere-induced new bone formation. After the three-dimensional reconstruction of the original image using CTvox software (SkyScan, Bruker), the CTAn software was used to calculate the quantitative data.

2.21. Histological analysis

At 7 days, 4 weeks, and 8 weeks after microsphere implantation, rats were euthanized. The skull was fixed in 4% paraformaldehyde and the bone tissue was embedded in paraffin after 45 days of decalcification, and sectioned with an electric microtome (Leica RM2016). The harvested sections were used for hematoxylin and eosin (H&E) staining, Masson trichrome staining, and immunofluorescence analysis.

2.22. Blood biochemical analysis

To assess the biosafety of the materials blood biochemical analysis was performed on rats. Before the rats were euthanized, the whole blood of the rats in each experimental group was collected through the tail vein blood collection method, and the upper serum was collected after centrifugation. Then, the blood biochemical analysis was performed with the liver function and kidney function assay kits.

2.23. Statistical analysis

The data in this paper were shown as mean ± standard deviation. GraphPad Prism 8.0 software was used for analyzing statistical significance and constructing graphs. Student's *t*-test was conducted to compare the statistical significance.

3. Results

3.1. Preparation and characterization of MPAH

We first synthesized MPAH according to the method reported in the literature [34]. Fig. 2A shows the preparation process of MPAH. First, the rigid template, monodisperse SiO_2 NPs, was synthesized by hydrolyzing TEOS. The SiO_2 NPs were mixed with $KMnO_4$ to prepare porous core-shell SiO_2@MnO_2 NPs. H–MnO_2 was prepared using Na_2CO_3 to dissolve SiO_2 to enhance the contact between MnO_2 and the medium. The MPAH was further obtained by electrostatic interaction of negatively charged H–MnO_2 with cationic PAH, which would be used for further experiments.

As shown in Fig. 2B–D, TEM images confirmed the successful synthesis of SiO_2 NPs, SiO_2@MnO_2 NPs, and H–MnO_2. With the dissolution of the SiO_2 template, an approximately 25-nm monolayer H–MnO_2 was obtained. Meanwhile, SEM elemental mapping showed that O and Mn elements were uniformly distributed on the H–MnO_2 surface (Fig. 2E). Furthermore, the successful synthesis of H–MnO_2 was further confirmed by the characteristic diffraction peaks of the XRD method (Fig. S1), and the two sub-peaks of Mn 2p1/2 (654.6 eV) and Mn 2p3/2 (642.9 eV) appeared in the XPS spectra (Fig. 2F and Fig. S2) [35,36]. Moreover, the results of nitrogen adsorption isotherms showed that H–MnO_2 had a large Brunauer–Emmett–Teller surface area, which would facilitate the reaction of H–MnO_2 with the medium and protein adsorption (Fig. 2G). According to Fig. 2H, the zeta potential results showed that H–MnO_2 was negatively charged. The MPAH obtained after PAH modification exhibited a positive charge, which would be more favorable for protein adsorption, which was verified by the adsorption experiments of the bovine serum albumin (BSA) model protein (Fig. S3). In addition, TEM images and dynamic light scattering (DLS) showed that the particle size was about 270 nm, and the morphology of MPAH after PAH modification was unchanged and uniformly distributed (Figs. S4 and S5).

3.2. Preparation and characterization of MPBP

As shown in Fig. 3A, MPAH was loaded with negatively charged protein, and the resulting MBP was mixed with PLGA to synthesize multi-functional MPBP using the emulsion technique. As shown in Fig. 3B, coil-like PLGA microspheres formed when the proportion of MPB was 10%, which would be unfavorable for sustained drug release. When the MPB ratios were 0.5%, 1%, 2.5%, and 5%, PLGA microspheres formed with smooth and dense surfaces, which would be beneficial to the sustained release of protein drugs, improving drug utilization. On

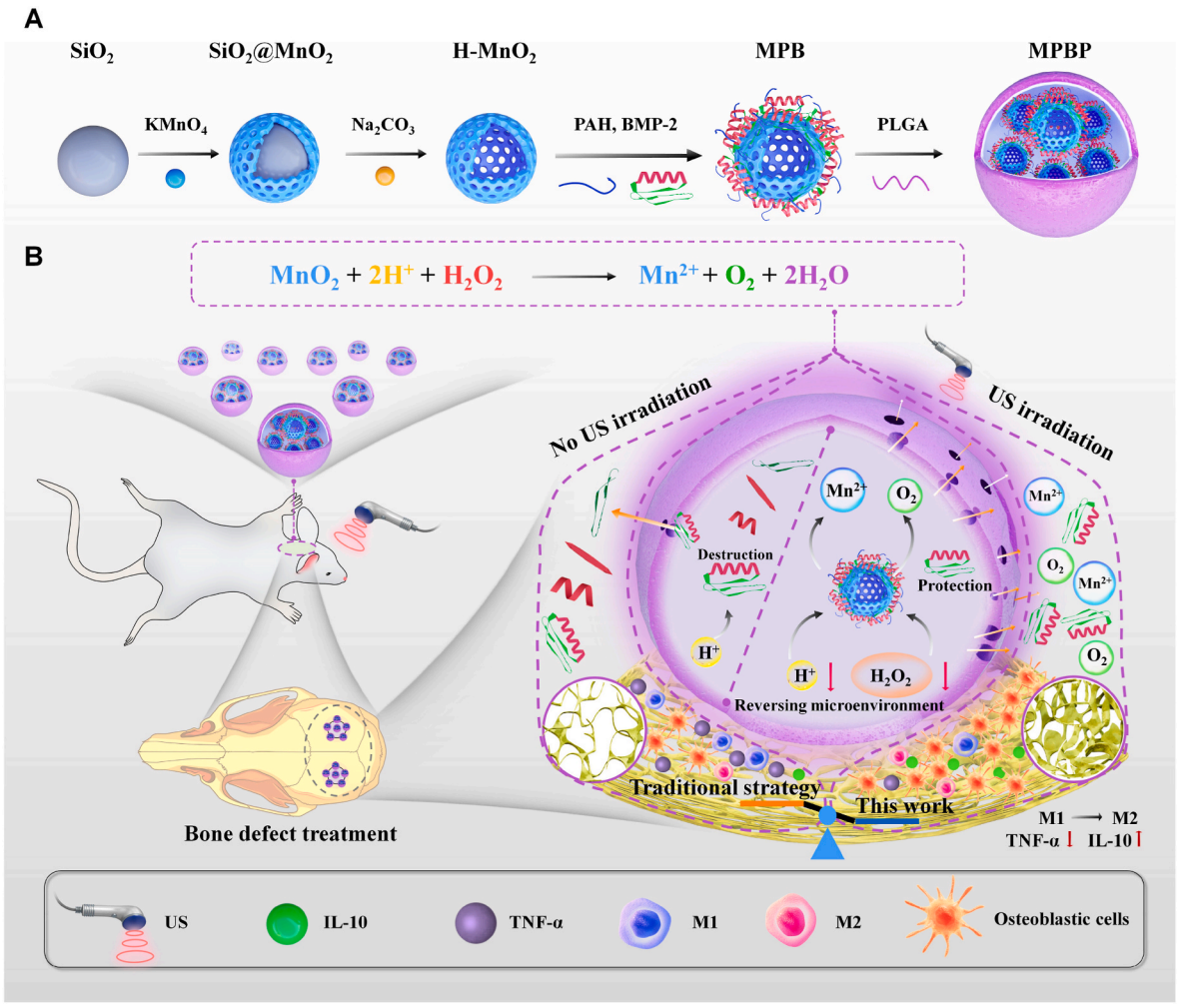

Fig. 1. Schematic diagram of the preparation and use of the multi-functional MPBP microsphere system for bone defect treatment with US and microenvironment dual response. MPBP protected BMP-2, reversed the bone injury microenvironment, and modulated the immune microenvironment to achieve bone defect repair under a combination of effects.

the other hand, protein and MnO_2 concentrations are crucial for repairing bone defects, while the protein content and the amount of Mn^{2+} are positively related. Therefore, we chose 5% as the optimal ratio based on the results of the Mn^{2+} loading rate and carried out subsequent experiments (Fig. 3C).

Next, we comprehensively evaluated the prepared MPBP. After labeling the BSA with Cy5, a fluorescence microscope showed that MPB was loaded inside PLGA (Fig. 3D), and the microsphere size was about 100 μm (Fig. 3E). Next, we tested the ability of Mn^{2+} and BSA model protein to be released from the microspheres under different conditions (Fig. 3F and G). First, we simulated the bone injury microenvironment with acidic and H_2O_2 overexpression and found that Mn^{2+} and BSA could be effectively released under a pH of 5.5. In addition, when the pH was 5.5, and H_2O_2 existed simultaneously, the release efficiency of Mn^{2+} and BSA were higher. However, under normal physiological conditions, the release of Mn^{2+} and BSA was slow, and the amount released was low, indicating that MPBP could be released responsively at the site of bone injury. In addition, when US irradiation was applied, the release of Mn^{2+} and BSA was further accelerated at pH = 5.5 and in the presence of H_2O_2. It was exciting that US irradiation could also control the release of contents on demand. This process could be interpreted as the acid-induced and H_2O_2-accelerated degradation of MnO_2 in the bone injury microenvironment, resulting in the generation of Mn^{2+}, the dissociation of BSA, and accelerated the release process of both under US irradiation [37]. Therefore, MPBP achieved intelligent and on-demand release under the dual response of the microenvironment and the US. In addition to the observation that MPBP could generate Mn^{2+} and release BSA, we also verified that MPBP reacted with acid and H_2O_2 to generate O_2 due to the presence of MnO_2, further improving the microenvironment of bone injury (Fig. 3H).

3.3. Properties of MPBP

We conducted SEM tests on the microspheres after the protein release experiment to better explain the dual-responsive release. As shown in Fig. 4A, the originally smooth microsphere surface with PLGA degradation developed pores over time, and larger holes formed on the surface when the US was applied. Compared with normal physiological conditions, MnO_2 degraded faster in response to acidic and H_2O_2-overexpressed bone injury microenvironment; therefore, more BSA and Mn^{2+} were released from the pores on the surface of MPBP. The surface porosity of MPBP further increased after the application of US irradiation, further facilitating the on-demand release of BSA and Mn^{2+}.

Since the acid produced by PLGA degradation will degrade the protein and reduce the therapeutic effect, we next evaluated the protective effect of MnO_2 on BMP-2. First, an acid-base test was performed to determine the acidity inside the PLGA microspheres and MPBP during degradation. Lysosensor yellow/blue® dextran probe is a specific acidic indicator that fluoresces blue under neutral conditions and yellow under acidic conditions. As shown in Fig. 4B, the images of the confocal laser

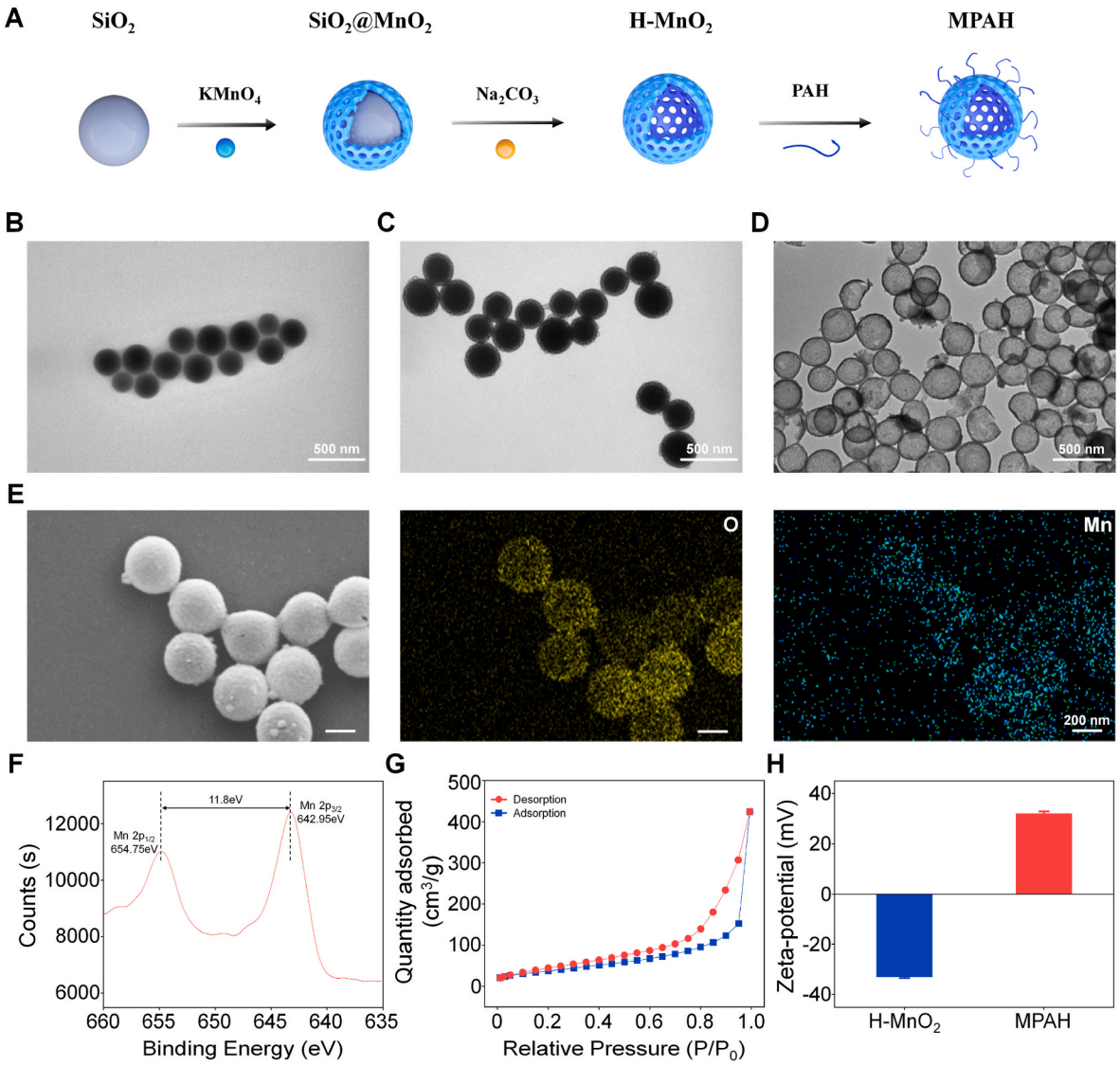

Fig. 2. Preparation and characterization of MPAH. (A) Schematic diagram of the preparation of MPAH. TEM images of (B) SiO_2, (C) SiO_2@MnO_2, and (D) H–MnO_2. (E) SEM images of H–MnO_2 and elemental mapping images of O and Mn of H–MnO_2. (F) XPS image of H–MnO_2. (G) Nitrogen adsorption isotherms of H–MnO_2.(H) Zeta-potential analysis of H–MnO_2 and MPAH. Data are shown as the mean ± SD (n = 3).

scanning microscope showed that the probe's fluorescence during MPBP degradation always appeared blue. In contrast, the probe within the PLGA microspheres gradually emitted yellow fluorescence over time, indicating that the PLGA slowly degraded over time to produce an acidic environment, and the MPBP neutralized the acid produced by degradation because of the presence of MnO_2. The simulation experiments were further performed to visually demonstrate the protective effect of MnO_2 on BMP-2. Three experimental groups, BMP-2, PBS (pH = 3) + BMP-2, and PBS (pH = 3) + BMP-2 + MnO_2, were set up. For the circular dichroism tests, the results showed that MnO_2 protected the secondary structure of BMP-2 (Fig. 4C). The results of mass spectrometry tests indicated that MnO_2 protected BMP-2 from destruction by the acid (Fig. 4D).

Overall, MnO_2 could consume the acid generated by PLGA degradation to protect BMP-2 from acid destruction. It could also consume H_2O_2 in the bone injury microenvironment to generate Mn^{2+} and O_2 to reverse the bone injury microenvironment, enhancing the osteogenic effect. In addition, the intelligent responsiveness of the microenvironment and the on-demand responsiveness of US irradiation would allow for the controlled release of MPBP contents. Therefore, multi-functional MPBP had a promising potential to promote bone defect repair (Fig. 4E).

3.4. Analysis of MPBP promoting cell proliferation, consuming ROS and polarizing macrophages

We studied MPBP in detail at the cellular level to demonstrate its potential in promoting bone defect repair. Firstly, we evaluated the biocompatibility of MPBP through cell experiments. As shown in Fig. 5A, after incubating MC3T3-E1 cells with MPBP extracts containing different proportions of MnO_2, the cell viability was >80%, indicating that MPBP had good biocompatibility and deserved further investigations. In the bone injury microenvironment, ROS will be produced, consisting mainly of H_2O_2, which will cause oxidative damage to cells after accumulation, leading to inflammation and affecting osteoblast proliferation. Therefore, we further investigated the ability of MPBP to consume ROS. As shown in Fig. 5B, CCK-8 analysis showed that the proliferation of MC3T3-E1 cells was not affected by MPBP and which could play an anti-oxidative role by consuming ROS to protect the normal proliferation of cells due to the efficient consumption of H_2O_2 by the presence of MnO_2 in MPBP (Fig. 5C and Fig. S6). Live/death staining analysis further proved that MPBP could resist oxidative damage and protect the normal proliferation of MC3T3-E1 cells, in agreement with the results of the CCK-8 analysis (Fig. 5D).

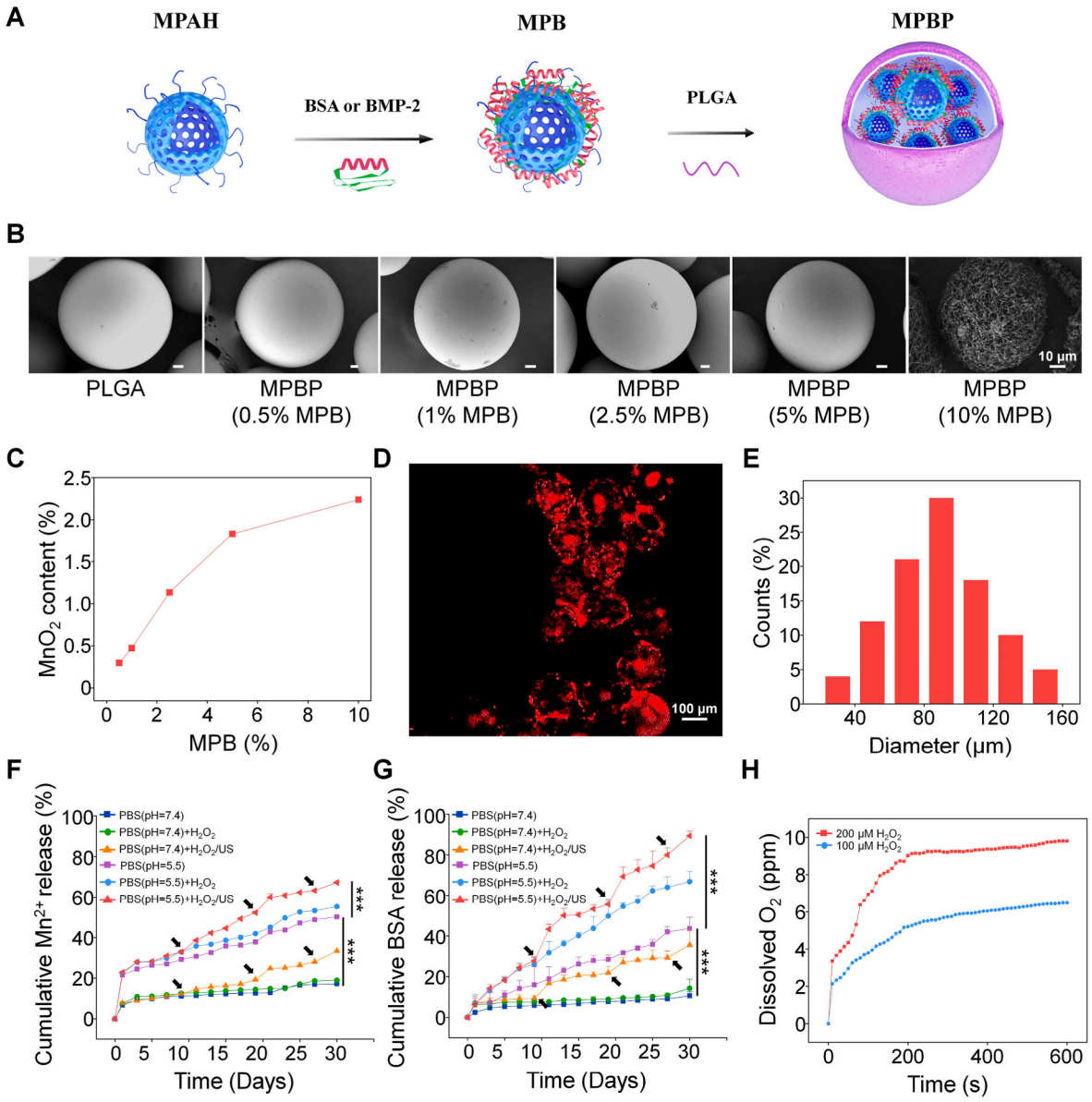

Fig. 3. Preparation of MPBP. (A) Schematic diagram of the preparation of MPBP. (B) SEM images of MPBP, which were prepared with different ratios of MPB and PLGA. (C) The MnO_2 content calculated from the Mn content measured by ICP test. (D) Fluorescence microscopy images of MPBP prepared by Cy5-labeled MPB with PLGA. (E) DLS analysis of MPBP prepared by 5% MPB and PLGA. The cumulative release profile of (F) Mn and (G) BSA from MPBP. (G) Dissolved oxygen release profiles of MPBP under different conditions. Data are shown as the mean ± SD (n = 3).

Studies have shown that the presence of ROS affects the polarization process of macrophages, which is critical for the repair of bone defects, so we wanted to assess, at the cellular level, whether MPBP could have an effect on macrophage polarization by depleting ROS. As shown in Fig. S7A, macrophages were incubated with LPS after applying different treatment processes, and then stained for iNOS which is the marker of M1-type macrophages. Furthermore, the expression of macrophage genes was quantitatively assessed by RT-qPCR. As shown in Figs. S7B–C, iNOS gene expression was significantly reduced in the MnO_2@PLGA, MPBP, and MPBP/US groups, whereas Arg-1 (arginine, an M2 marker) gene expression was significantly increased. These results illustrated that with the introduction of MnO_2, the clearance of ROS prompted macrophage polarization from M1 to M2. It demonstrated the potential of MPBP to modulate the immune microenvironment at the site of bone defects. Altogether, MPBP not only had good biocompatibility but also consumed ROS due to the presence of MnO_2 which played the role of antioxidant defense, helping reverse the microenvironment of bone injury, promoting the proliferation of osteoblasts, polarizing macrophages, and enhancing bone repair.

3.5. *Analysis of the osteogenic effect of MPBP*

ALP staining, ARS staining, and the expression of osteogenesis-related genes were performed to further investigate the *in vitro* osteogenic activity of MPBP. As shown in Fig. 6A–C, in comparison with the control group, the MnO_2@PLGA group could release Mn^{2+} and O_2 to promote osteoblast proliferation due to the presence of MnO_2, and the BMP-2@PLGA group promoted osteoblast proliferation due to the presence of BMP-2, resulting in increased ALP expression in both groups. MPBP could significantly increase ALP expression compared to the control group due to MnO_2 neutralizing the acidity generated by PLGA degradation to protect BMP-2 from degradation and the responsive release of BMP-2, Mn^{2+}, and O_2. In addition, since US irradiation could promote the release of contents, the expression of ALP in the MPBP/US

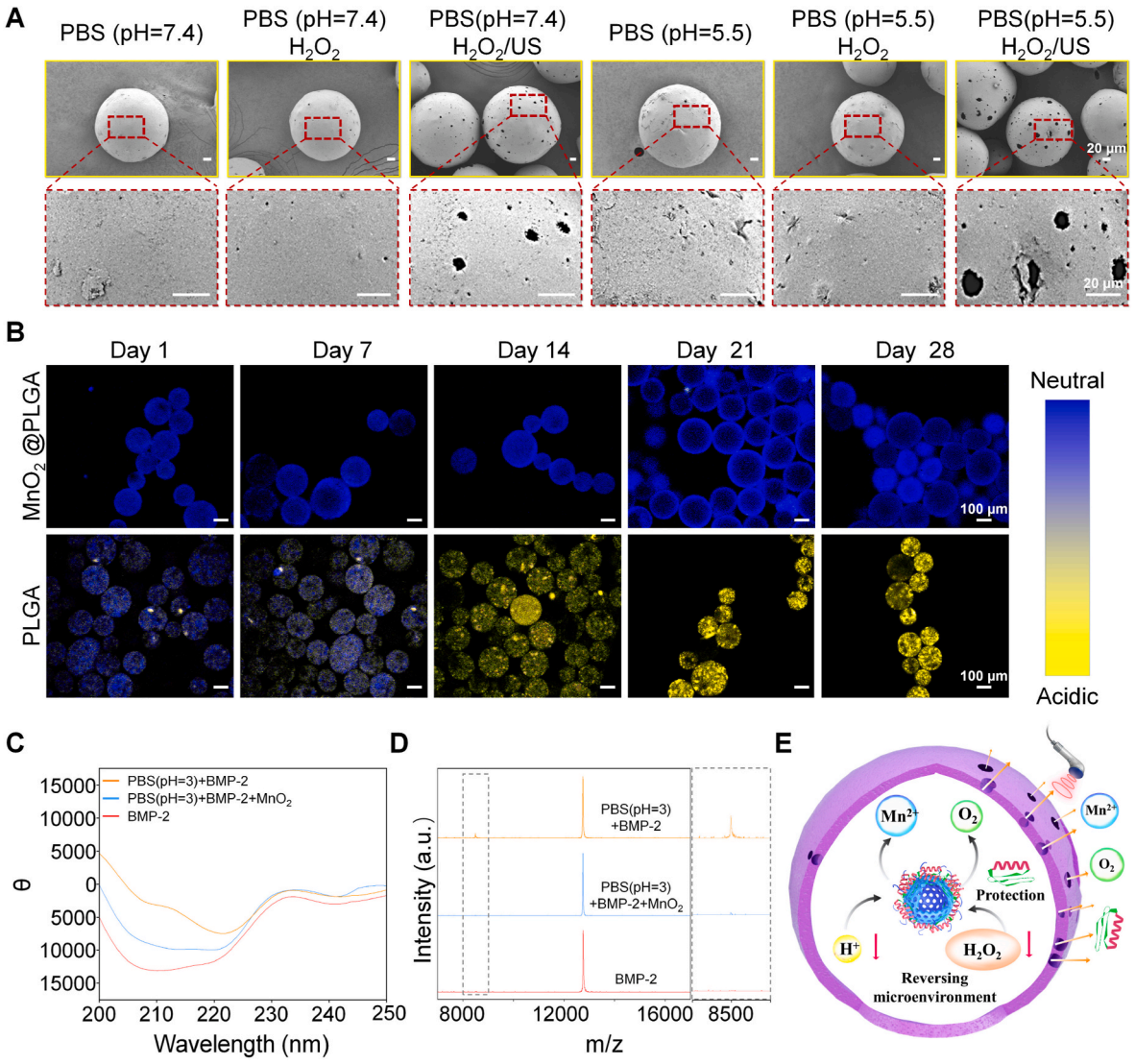

Fig. 4. Properties of MPBP. (A) SEM images of MPBP under different conditions after 30 days. (B) Fluorescence microscopy images of PLGA microspheres and MPBP after loading Lysosensor yellow/blue® dextran probe. Excitation: 364 nm. (C) Circular dichroism curves of BMP-2 under different conditions. (D) Mass spectrometry analysis of BMP-2 under different conditions. (E) Schematic diagram of MPBP used to protect BMP-2 and release contents by the dual response.

group was further upregulated. Meanwhile, ARS staining also yielded similar results, with the MPBP/US group exhibiting the most abundant calcium deposition compared to the other groups. The expression of osteogenic genes was quantitatively assessed by RT-qPCR and the primer sequences for each gene were listed in Table S1. As shown in Fig. 6D–G, because of the combined action of MnO_2, BMP-2, and US, the MPBP/US group could significantly promote the expression of osteogenesis-related genes osteopontin (OPN) and runt-related transcription factor 2 (Runx2). Moreover, the MPBP/US group exhibited significant upregulation of the osteogenic differentiation genes, osteocalcin (OCN), and collagen I (Col-I). Altogether, since MnO_2 could neutralize the acid produced by PLGA degradation to protect BMP-2 and the responsive release of BMP-2, Mn^{2+}, and O_2 coupled with US irradiation to promote the release of the contents, MPBP/US exhibited excellent *in vitro* osteogenic activity.

3.6. MPBP promoted the repair of bone defects

Encouraged by the above-mentioned favorable *in vitro* osteogenic outcomes, the effectiveness of MPBP for *in vivo* bone defect repair was evaluated. Firstly, the introduction of MnO_2 into PLGA microspheres to protect bioactive proteins within the microspheres was analyzed. As shown in Fig. S8A, microspheres containing the acidic indicator were implanted into rats with two circular skull bony defects, and the yellow fluorescence within the PLGA microspheres gradually increased with time, which indicated that PLGA produces an acidic environment *in vivo* after degradation begins. However, a neutral environment was maintained within the microspheres of the MnO_2@PLGA group, suggesting that the introduction of MnO_2 neutralized the acid produced by PLGA degradation. Next, EGFP was chosen as a model protein to demonstrate the protective effect of MnO_2 on bioactive proteins. EGFP was loaded into different microspheres implanted into rats with two circular skull bony defects, and the green fluorescence signals inside the PLGA microspheres were significantly weakened with time, while there was no significant change in the green fluorescence signals inside the microspheres in the MnO_2@PLGA group. These results illustrated that the acid generated within the PLGA microspheres caused damage to the structure of EGFP, while MnO_2 was able to neutralize the acid and protect EGFP (Fig. S8B). Together, the above experiments demonstrated that MnO_2 in MPBP had a protective effect on bioactive proteins *in vivo*. Then, rats with two circular skull bony defects were randomly assigned to seven groups: PBS, US, PLGA, MnO_2@PLGA, BMP-2@PLGA, MPBP, and

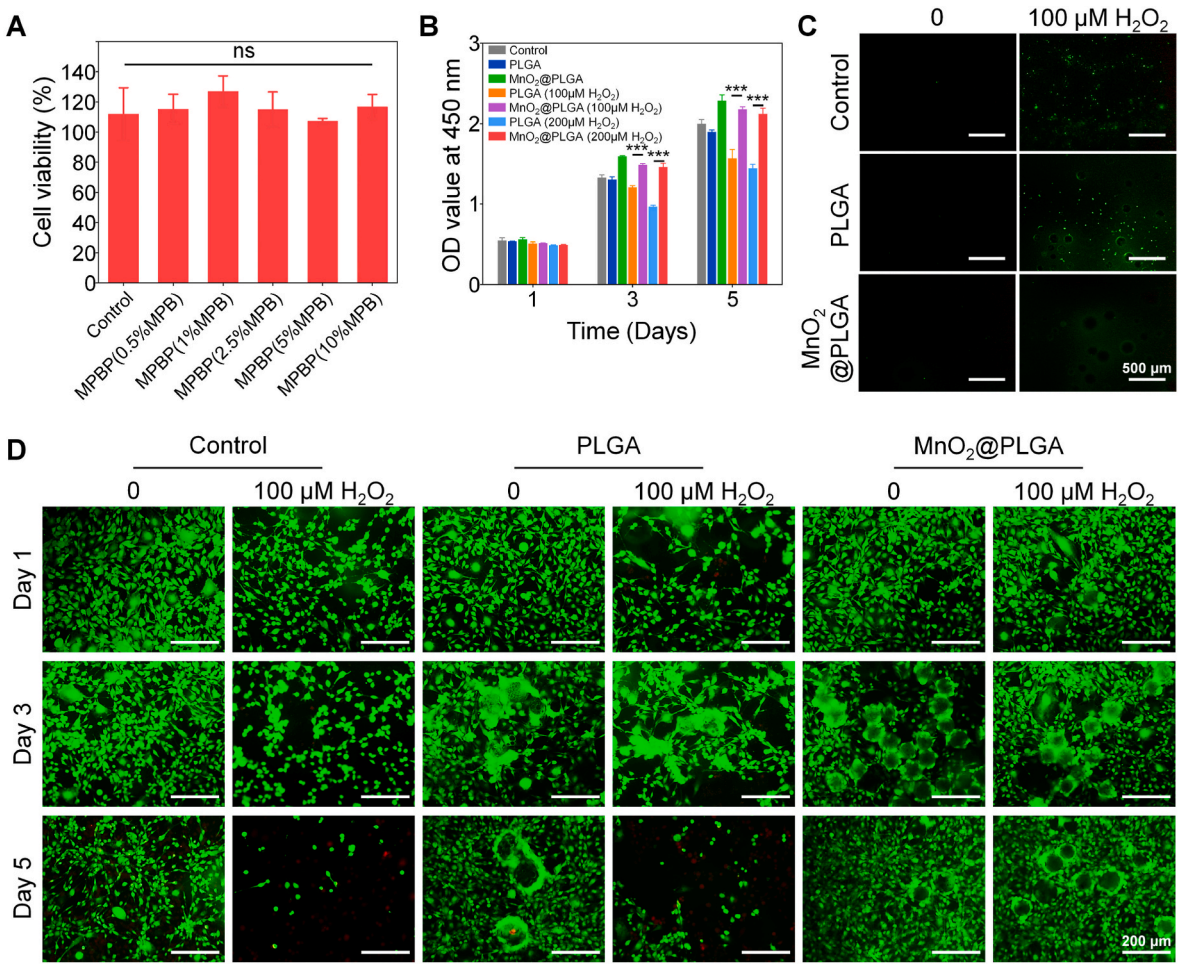

Fig. 5. Analysis of MPBP promoting cell proliferation and consuming ROS. (A) CCK-8 analysis of MPBP extracts with different MnO_2 contents after incubation with cells. (B) Proliferation analysis of cells after different treatments. (C) Fluorescence microscopy images of DCFH-DA-stained MC3T3-E1 cells after different treatments. (D) Fluorescence microscopy images of MC3T3-E1 cells stained with propidium iodide and calcein-AM after different treatments. Data are shown as the mean ± SD (n = 3).

MPBP/US. As shown in Fig. 7A, when the implantation of each microsphere was finished, US irradiation treatment was performed weekly, and the osteogenic repair effect was analyzed in the fourth and eighth weeks. After different treatments, the new bone formation was assessed using computed tomography analyses. As shown in Fig. 7B, representative three-dimensional images of the newly formed bone tissue were reconstructed with Micro-CT. New bone growth from the edges of the defect toward the central area was observed in both experimental groups compared to the control group over time. There was a significant increase in the volume of new bone in the MnO_2@PLGA group in comparison to the control group, indicating that the presence of MnO_2 in PLGA could consume the H_2O_2 produced at the site of bone injury, reversing the microenvironment while promoting osteoblast proliferation because of the release of Mn^{2+} and O_2, which combine to provide a moderate bone repair effect. The BMP-2@PLGA group also showed a significant bone repair effect compared to the control group because BMP-2 in PLGA for sustained release could also promote bone regeneration to a certain extent. The bone defect repair effect in the MPBP group was obviously better than that in the MnO_2@PLGA and BMP-2@PLGA groups, indicating that introducing both MnO_2 and BMP-2 into PLGA microspheres could provide a better bone repair effect because MnO_2 could neutralize the acid produced by PLGA degradation to protect the structure of BMP-2 while releasing BMP-2, Mn^{2+}, and O_2 responsively. Therefore, it could better promote the proliferation of osteoblasts. In addition, the release of MPBP contents could be further increased on-demand after US irradiation application, significantly increasing the volume of new bone in the MPBP/US group. In addition, the quantitative results of Micro-CT showed that the MPBP/US group had higher bone volume/tissue volume (BV/TV), trabecular number (Tb.N), and trabecular thickness (Tb.Th) than the control group and trabecular separation (Tb.Sp) was lower than the control group. It could also be seen that the MPBP/US group had an obvious increase in BV/TV and Tb.N compared with the MPBP group, indicating that MPBP combined with US irradiation had the best osseointegration ability and could promote osteogenesis (Fig. 7C–E and Fig. S9).

3.7. Histological analysis

Furthermore, H&E and Masson trichrome staining were used to study new bone formation at the area of bone defects to further demonstrate the role of MPBP in promoting osteogenesis. In Fig. 8A and 8B, the star represents the microspheres, the triangle represents the new bone, and the dashed box represents the defect area. The results showed no new bone formation in the control group, which was mostly fibrous connective tissue. In contrast, all the experimental groups showed new bone growth from the edge of the defect to the central area. Since MnO_2 could neutralize the acid produced by PLGA degradation to protect the structure of BMP-2 while responsively releasing BMP-2, Mn^{2+}, and O_2, this would better promote osteoblast proliferation, with the best osteoinduction and osseointegration ability in the MPBP/US group.

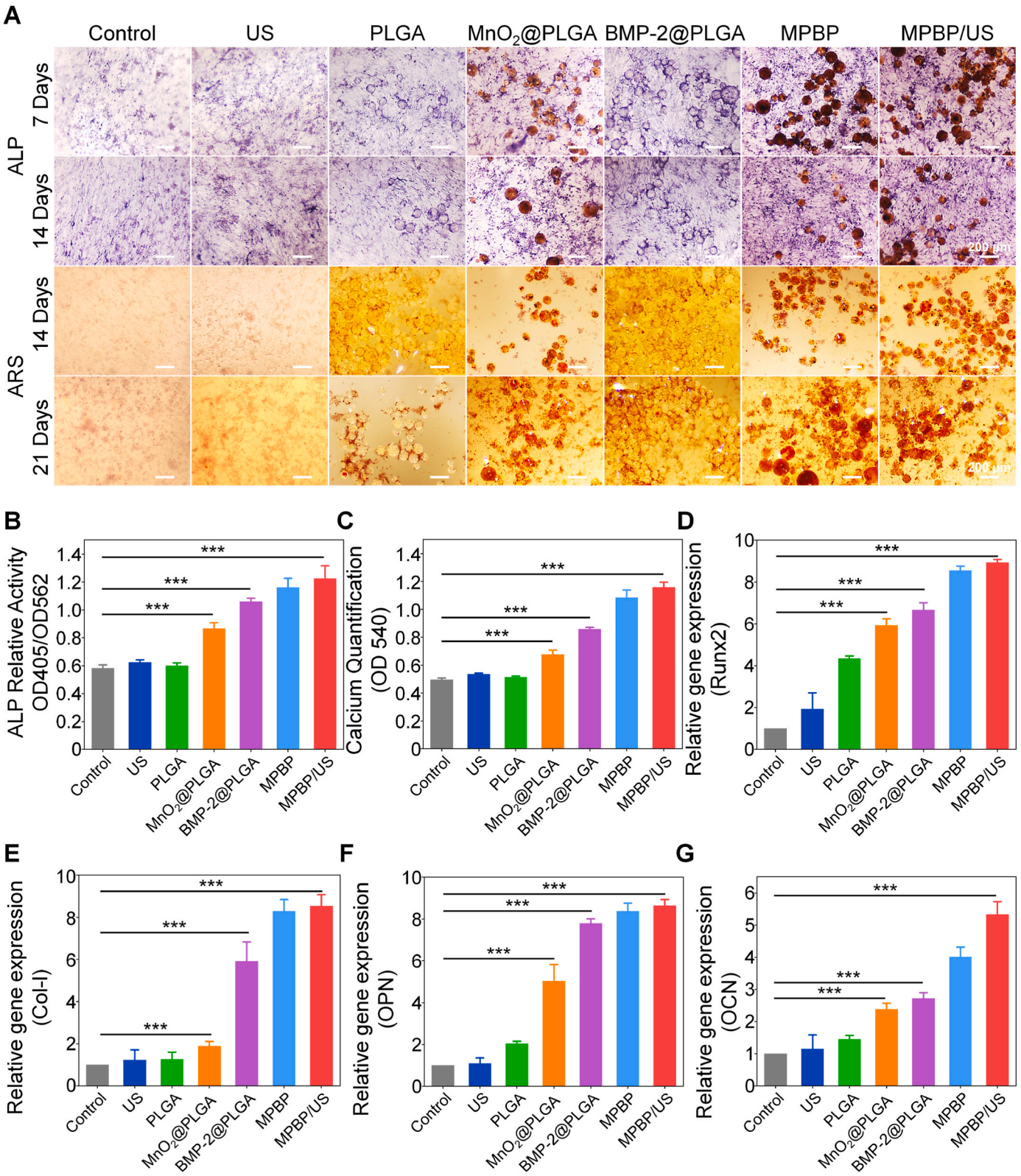

Fig. 6. Analysis of the osteogenic effect of MPBP. (A) Microscopic images of ALP and ARS staining of MC3T3-E1 cells after different treatments. Quantitative analysis of (B) ALP staining and (C) ARS staining. Expression analysis of osteogenic-related genes (D) Runx2, (E) Col-I, (F) OPN, and (G) OCN. Data are shown as the mean ± SD (n = 3).

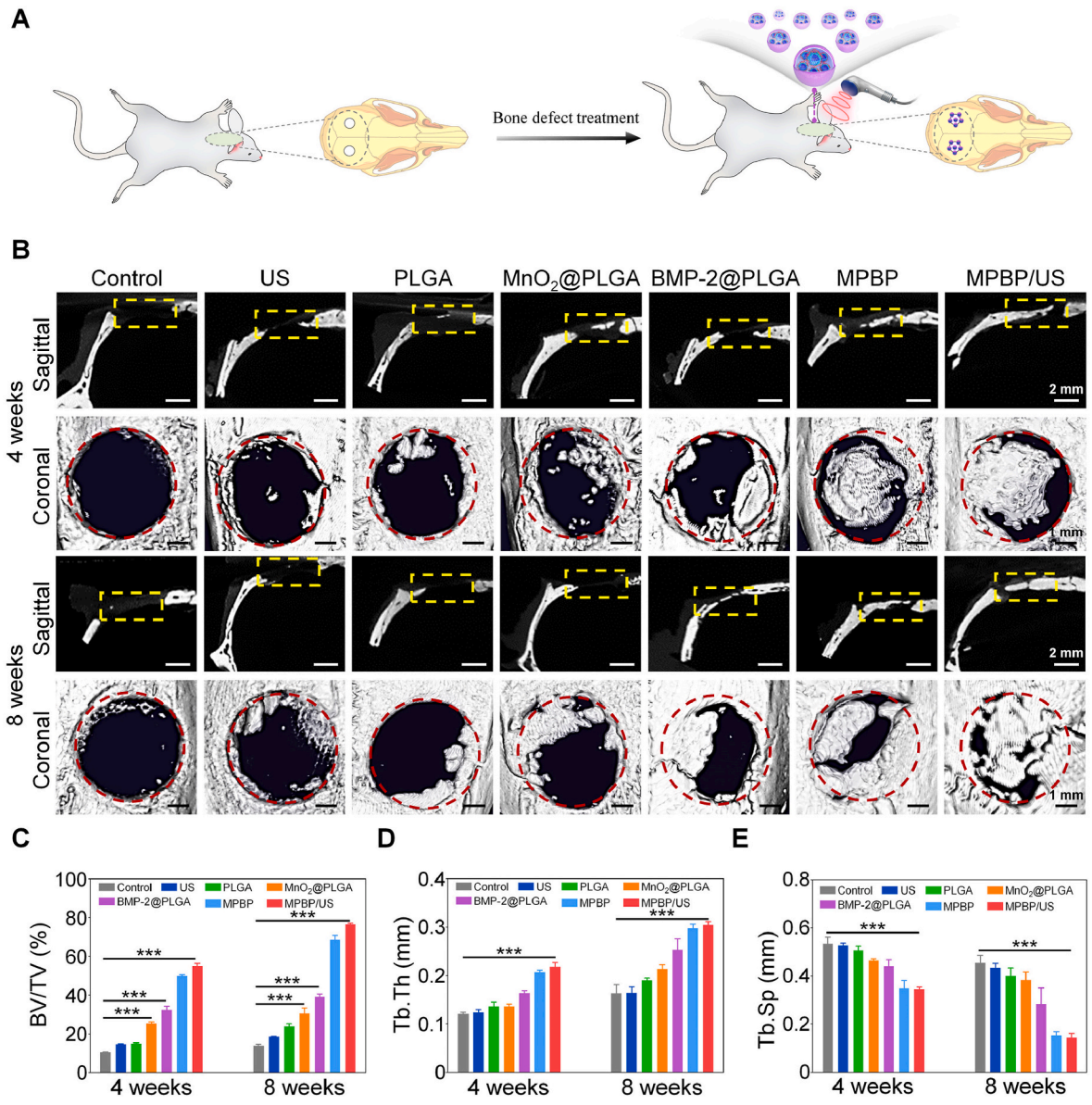

Fig. 7. MPBP promoted the repair of bone defects. (A) Schematic diagram of MPBP for bone defect repair. (B) Micro-CT reconstruction images of coronal and sagittal at weeks 4 and 8 after different treatments. Quantitative analysis of (C) BV/TV, (D) Tb.Th, and (E) Tb.Sp. BV/TV: Bone volume/total volume; Tb.Th: Trabecular thickness; Tb.Sp: Trabecular separation analysis. Data are shown as the mean ± SD (n = 3).

Moreover, we observed that cells had entered the microspheres to form fibrous tissues as a potential immature bone matrix, suggesting that MPBP could have long-term osteogenic activity by promoting cell adhesion and proliferation to bridge the gap at the defect sight.

Altogether, the Micro-CT and histological analysis results showed that MPBP in combination with US irradiation could significantly promote bone repair, with the highest volume of new bone in all experimental groups, with long-term osteogenic activity, because MPBP provided a site for osteoblast adhesion and MnO_2 neutralized the acid produced by PLGA degradation to protect BMP-2 from acid degradation, allowing it to maintain long-term biological activity and further proliferation of osteoblasts. In addition, MnO_2 further eliminated ROS from the bone injury microenvironment to protect cells against oxidative damage. It promoted cell growth by releasing Mn^{2+} and O_2, which reversed the bone injury microenvironment and enhanced the osteogenic effect. Furthermore, MPBP had micro-environment intelligent responsiveness and US irradiation on-demand responsiveness to avoid burst release and non-release of the contents. That is why multifunctional MPBP microspheres had such excellent bone defect repair ability.

3.8. Regulation of the immune microenvironment by MPBP

Bone defect repair is accompanied by an injury-regeneration, inflammation-repair process; therefore, the effect is closely related to the immune microenvironment and the bone injury microenvironment. Heterogeneous macrophages play a key part in the bone injury process. The presence of acid and hypoxia in the bone injury microenvironment will lead to the persistence of inflammation, affecting the conversion of M1 to M2. Moreover, ROS is an important mediator of M1 polarization and can promote M1 polarization through the NF-κB pathway. Therefore, the bone injury microenvironment also affects the immune microenvironment. In the above experiments, we verified that MPBP could regulate the bone injury microenvironment, remove ROS, neutralize the acidic environment, and improve the hypoxic environment to achieve perfect bone defect repair. We aimed to verify whether

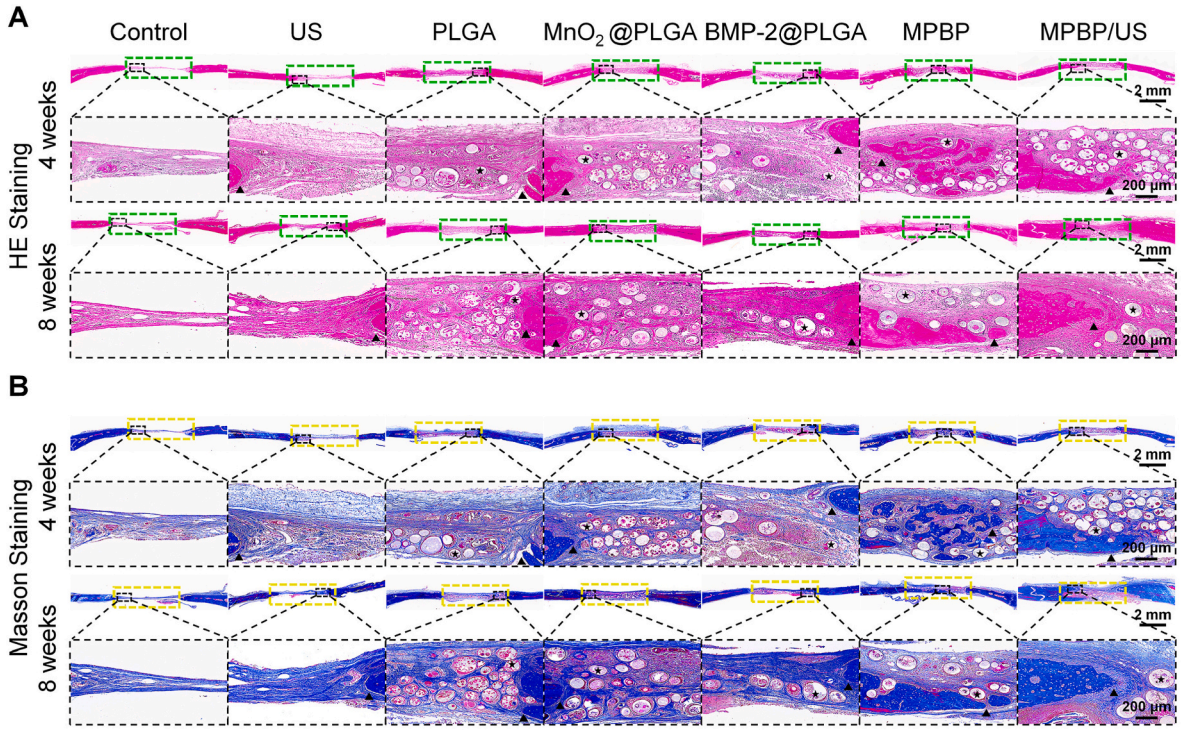

Fig. 8. Histological analysis. (A) H&E staining and (B) Masson trichrome staining of the bone defect site after different treatments. The star represented the microspheres, the triangle represented the new bone, and the dashed box represented the defect area.

immune microenvironment regulation was involved in this process. We further studied the underlying mechanisms of MPBP in promoting bone repair.

As shown in Fig. 9A–C, the expression of inflammatory factors was studied by immunofluorescence staining. The expression of pro-inflammatory factor TNF-α was significantly downregulated in the MnO_2@PLGA, MPBP, and MPBP/US groups compared with the control group. In contrast, the expression of the anti-inflammatory factor IL-10 was significantly upregulated, indicating that PLGA loaded with MnO_2 improved the immune microenvironment after the reversal of bone injury microenvironment, such as ROS overexpression, acidity, and hypoxia, with no chronic inflammation development.

Immunofluorescence staining was also used to assess the polarization of macrophages. As shown in Fig. 9D–F and Fig. S10, the MnO_2@PLGA, MPBP, and MPBP/US groups exhibited weaker iNOS specific fluorescence, and stronger Arg1 specific fluorescence compared with the control group signal, and the Arg1 specific fluorescence continued to increase with time, suggesting that MnO_2-loaded PLGA promoted the conversion of M1 to M2, which is directly related to the NF-κB pathway inhibition by MnO_2 scavenging ROS in addition to the elimination of the inflammatory environment. Therefore, MPBP reversed the bone injury microenvironment, promoted osteoblast proliferation, and improved the immune microenvironment in the bone repair process. It was under the coordination of these various functions that the perfect bone repair effect was realized.

3.9. The biosafety analysis of MPBP

The biosafety of MPBP was also evaluated. As shown in Fig. S11, first, we recorded the body weight of each group of rats during the treatment. The rats' body weight did not change significantly after microsphere implantation and treatment and was in a stable growth state, indicating that MPBP had excellent biocompatibility. In addition, blood from each group of rats was collected for blood biochemical analysis at the end of the treatment. As shown in Fig. S12, there were no obvious changes in any blood biochemical parameters after microsphere implantation and at the end of treatment, indicating that MPBP did not have long-term toxicity. Overall, the above experiments demonstrated that this multi-functional MPBP had excellent biosafety for bone defect repair.

4. Discussion

Bone tissue engineering is currently considered to be the most promising therapeutic approach for the treatment of bone defects, in which growth factor-based therapies are considered to be the most effective strategy for inducing tissue regeneration. BMP-2 is widely used but the use of a suitable carrier for delivery while controlling the release of the protein is crucial to achieve good bone repair results.

After a bone injury, the injury site usually becomes hypoxic, acidic, and enriched with reactive oxygen species forming a special bone injury microenvironment. Oxygen tension decreases from 22 mm Hg to 10 mm Hg between days 3 and 7 after fracture and gradually returns to 20 mmHg on day 42 of healing [38]. The pH of the fracture site was measured in experimental animals in earlier studies, and the fracture site varied from 4.2 to 7.19 at different time points [18]. All of these factors can adversely affect the repair of bone tissue. In addition, the bone injury microenvironment produces a sustained inflammatory response that affects macrophage polarization, creating an immune microenvironment that is even less conducive to bone injury repair. Therefore, in summary, the treatment of bone defects requires comprehensive consideration from various aspects, and it is difficult for the traditional single-treatment strategy to play a sufficiently strong therapeutic role.

In this study, to better achieve the repair of bone defects, we decided to look for a repair solution that could simultaneously achieve therapy, reverse the bone injury microenvironment, and modulate the immune microenvironment after considering the complexity of the bone defect site.

The use of PLGA microspheres as carriers for the delivery of bioactive substances because of their biocompatibility and slow release has been widely reported, and they are ideal candidates for the delivery of BMP-2.

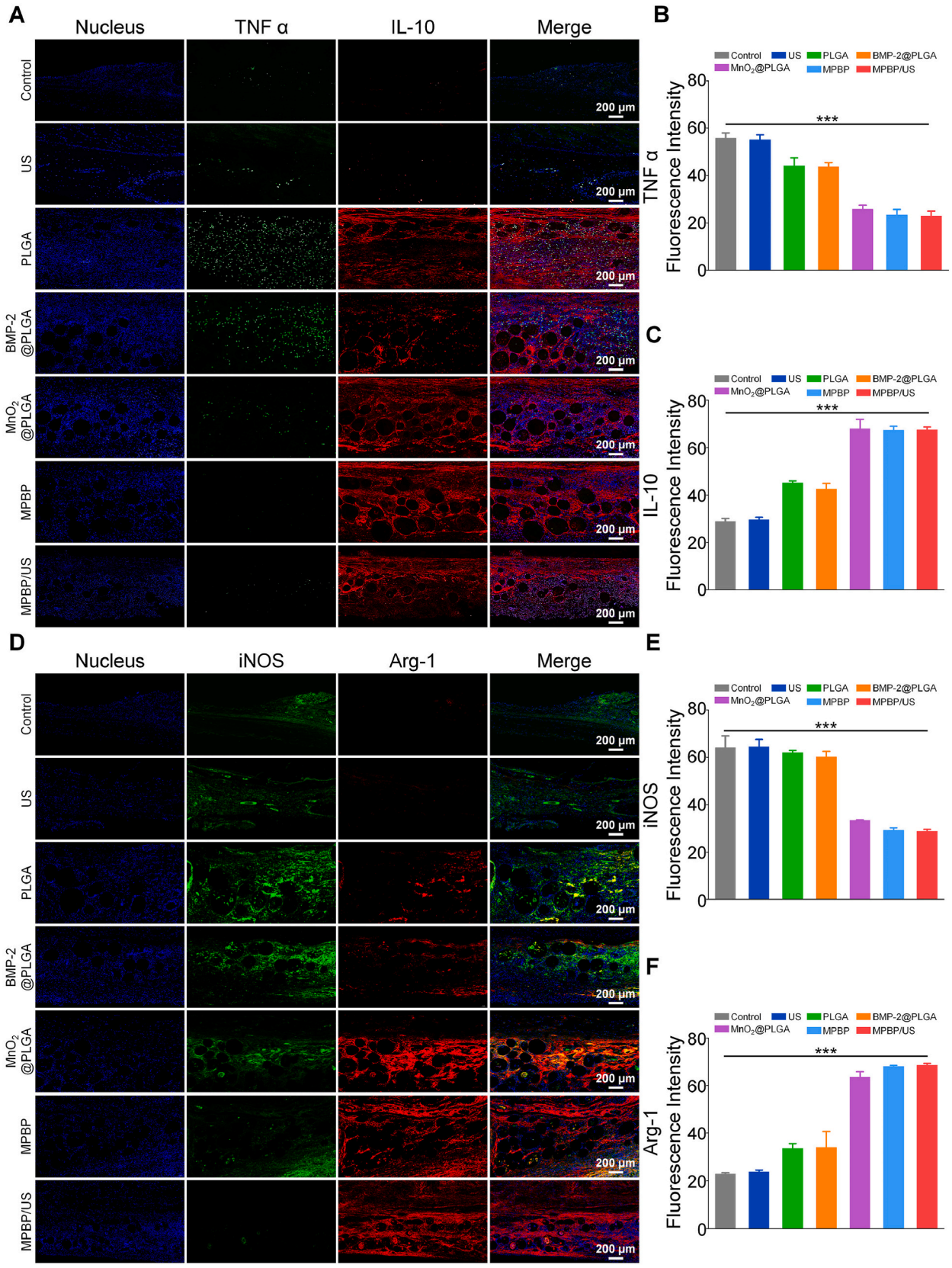

Fig. 9. Regulation of the immune microenvironment by MPBP. (A) Immunofluorescence staining images of TNF-α and IL-10 at the site of bone defects with different treatments. Quantitative analysis of (B) TNF-α, (C) IL-10 in Figure (A). (D) Immunofluorescence staining images of INOS and Arg1 at the site of the bone defect with different treatments after microsphere implantation 7 days. Quantitative analysis of (E) INOS, (F) Arg1 in (D). Data are shown as the mean ± SD (n = 3).

However, we note that the acidic conditions generated by PLGA degradation products can have a damaging effect on the bioactive substances. To overcome this drawback, we have prepared composite microspheres by cleverly introducing MnO_2 in PLGA microspheres in this work. We have demonstrated by both *in vitro* and *in vivo* simulation experiments (Fig. 4B–D and Fig. S8) that the introduction of MnO_2 can neutralize the acid produced by PLGA and protect the structure of BMP-2 from disruption, which will establish a promising foundation for the repair of bone defects. In addition, the introduction of MnO_2 scavenges ROS in the bone injury microenvironment (Fig. 5C) while generating Mn^{2+} and O_2 that are favorable for bone growth [39–41]. These will promote the expression of osteogenic genes and facilitate osteoblast proliferation (Fig. 6A–G). Importantly, we also demonstrated at the *in vitro* level that modulation of the immune microenvironment by scavenging ROS could promote the polarization of M1 macrophages towards M2 macrophages (Fig. S7). We expect this multi-functional microsphere system to achieve excellent bone defect repair results *in vivo* through preliminary experimental validation.

In order to investigate the osteogenic properties of the multi-functional microsphere system in detail, we established different experimental groups including PBS, US, PLGA, MnO_2@PLGA, BMP-2@PLGA, MPBP, and MPBP/US. The MnO_2@PLGA group was designed to assess the effect of bone defect repair by reversing the bone injury microenvironment and modulating the immune microenvironment. The BMP-2@PLGA group was a BMP-2 delivery scheme for traditional policies. The MPBP group could be regarded as a combined treatment group of MnO_2@PLGA and BMP-2@PLGA, which could verify the positive effect of protecting the structure of BMP-2 and the improvement of the microenvironment. The MPBP/US group was designed to further validate the effects of US-induced gain from on-demand, increased content release. Through the reconstructed images and quantitative analyses of Micro-CT, we saw a significant increase in BV/TV, Tb.Th and Tb.N, and a significant decrease in Tb.Sp in the MPBP/US group, which demonstrated that this multi-functional microsphere system could achieve excellent bone defect repair *in vivo* after combining multiple treatment strategies (Fig. 7B–E and Fig. S9). It is noteworthy that there was no significant difference between the MPBP group and the MPBP/US group in the comparison of data on Tb.Th and Tb.Sp. This may be due to the fact that the process of repairing bone defects is a complex and sophisticated process, while the increase in Tb.Th and decrease in Tb.Sp usually occurs in the following stages of bone repair. It requires continuous bone remodeling to achieve. Therefore, a long period of continuous observation may be needed to show more clearly the effect of US on Tb.Th and Tb.Sp. In addition to assessing the bone repair effect, we also evaluated the modulation of the immune microenvironment by MPBP at the *in vivo* level and showed that MPBP not only promoted the polarization of M1 to M2 macrophages but also significantly reduced the inflammatory response at the site of the bone defect. This suggests that the reversal of the bone injury microenvironment can modulate the immune microenvironment in a positive direction (Fig. 9 and Fig. S10).

Bone defect repair materials that can achieve clinical application require not only excellent repair performance but also good biosafety. BMP-2, MnO_2, and PLGA have been studied extensively in the field of biomaterials due to their biosafety. Multi-functional microsphere systems prepared using these materials have demonstrated excellent bone defect repair capabilities as well as not leading to systemic toxicity over a long period of time. This undoubtedly provides the strongest foundation for its clinical application. We also recognize that the initial concept of the multi-functional microsphere system leaves much to be desired. For example, individual microsphere systems have the potential for displacement at the site of a bone defect, and the mechanical properties of microspheres are weak, which makes them unsuitable for application in areas of weight-bearing. So, if it can be combined with hydrogel or used with scaffolding materials, it will further improve the utility of the treatment. We hope to obtain a bone defect repair material that can be used in clinical applications after combining excellent therapeutic effects, biosafety, and practicality.

5. Conclusion

US application and microenvironmental dual-responsive multi-functional microsphere system were prepared for on-demand controlled release of BMP-2 to reverse the bone injury microenvironment and regulate the immune microenvironment for bone defect repair, which resulted in excellent therapeutic outcomes in animal models of bone defects. We introduced MnO_2 to prevent damage to the BMP-2 structure caused by the internal acidic environment when PLGA delivered BMP-2. Firstly, hollow MnO_2 was prepared to increase the microenvironmental response efficiency. After cationization, H–MnO_2 was shown to be loaded with more BMP-2. MPB and PLGA were used to prepare MPBP microspheres by the S/O/W emulsion technique. MPBP had microenvironmental responsiveness to achieve BMP-2 dissociation and Mn^{2+} and O_2 production and could release the contents on-demand under the effect of US irradiation. Introducing MnO_2 not only neutralized the acid produced by microsphere degradation and protected the structure of BMP-2 but also scavenged H_2O_2, resolved hypoxia, generated Mn^{2+}, reversed the microenvironment of bone injury, increased the expression of osteogenic-related genes, OPN, Runx2, OCN, and Col-I, and promoted the proliferation of osteoblasts.

In addition, since the clearance of H_2O_2 and the reversal of the bone injury microenvironment promoted the polarization of M1 macrophages to M2 macrophages, it decreased the secretion of the pro-inflammatory factor TNF-α at the injury site and increased the expression of the anti-inflammatory factor IL-10, which decreased the inflammation at the injury site and regulated the immune microenvironment. Under the cumulative effect, multi-functional MPBP achieved excellent bone defect repair in a rat model of skull defects. This microsphere system, which combined on-demand delivery, reversed the bone injury microenvironment, modulated the immune microenvironment, and provided a new reference for clinical applications of protein delivery and bone defect repair.

Ethics approval and consent to participate

All animal studies were carried out according to the guidelines approved by the Animal Welfare and Ethics Committee of Changchun Institute of Applied Chemistry, Chinese Academy of Sciences.

CRediT authorship contribution statement

Qingxu Song: contributed to the experimental planning, performed the experiments, Formal analysis. **Dianwei Wang:** contributed to the experimental planning, performed the experiments, Formal analysis. **Haoyu Li:** Supervision, contributed to the intellectual input. **Zongliang Wang:** Supervision, contributed to the intellectual input. **Songjia Sun:** Supervision, contributed to the intellectual input. **Zhenyu Wang:** Supervision, contributed to the intellectual input. **Yi Liu:** Supervision, contributed to the intellectual input. **Sien Lin:** Supervision, contributed to the intellectual input. **Gang Li:** Supervision, contributed to the intellectual input. **Shaokun Zhang:** Supervision, founded the project, contributed to the experimental planning, intellectual input, Writing – review & editing. **Peibiao Zhang:** Supervision, founded the project, contributed to the experimental planning, intellectual input, Writing – review & editing.

Declaration of competing interest

The authors declare no competing financial interest.

Acknowledgements

The authors are thankful to the National Natural Science Foundation of China (82272468, 52173146), the Special Fund for Industrialization of Science and Technology Cooperation between Jilin Province and Chinese Academy of Sciences (2022SYHZ0022), and the Jilin Provincial science and technology development program (No.20230401089YY). In Fig. 1, some elements are created with BioRender.com.

Appendix A. Supplementary data

Supplementary data to this article can be found online at https://doi.org/10.1016/j.bioactmat.2023.10.007.

References

[1] A. Salhotra, H.N. Shah, B. Levi, M.T. Longaker, Mechanisms of bone development and repair, Nat. Rev. Mol. Cell Biol. 21 (11) (2020) 696–711.
[2] H. Sun, J. Xu, Y. Wang, S. Shen, X. Xu, L. Zhang, Q. Jiang, Bone microenvironment regulative hydrogels with ROS scavenging and prolonged oxygen-generating for enhancing bone repair, Bioact. Mater. 24 (2023) 477–496.
[3] P. Feng, R. Zhao, W. Tang, F. Yang, H. Tian, S. Peng, H. Pan, C. Shuai, Structural and functional adaptive artificial bone: materials, fabrications, and properties, Adv. Funct. Mater. (2023), 2214726.
[4] M. Bhandari, M. Swiontkowski, Management of acute hip fracture, N. Engl. J. Med. 377 (21) (2017) 2053–2062.
[5] M.-M. Germaini, S. Belhabib, S. Guessasma, R. Deterre, P. Corre, P. Weiss, Additive manufacturing of biomaterials for bone tissue engineering–A critical review of the state of the art and new concepts, Prog. Mater. Sci. 130 (2022), 100963.
[6] F.K. Lewns, O. Tsigkou, L.R. Cox, R.D. Wildman, L.M. Grover, G. Poologasundarampillai, Hydrogels and bioprinting in bone tissue engineering: creating artificial stem-cell niches for in vitro models, Adv. Mater. (2023), 2301670.
[7] Z. Jia, X. Xu, D. Zhu, Y. Zheng, Design, printing, and engineering of regenerative biomaterials for personalized bone healthcare, Prog. Mater. Sci. (2023), 101072.
[8] G.L. Koons, M. Diba, A.G. Mikos, Materials design for bone-tissue engineering, Nat. Rev. Mater. 5 (8) (2020) 584–603.
[9] S.S. Lee, X. Du, I. Kim, S.J. Ferguson, Scaffolds for bone-tissue engineering, Matter 5 (9) (2022) 2722–2759.
[10] B.H. Shan, F.G. Wu, Hydrogel-based growth factor delivery platforms: strategies and recent advances, Adv. Mater. (2023), 2210707.
[11] Y. Miao, Y. Chen, J. Luo, X. Liu, Q. Yang, X. Shi, Y. Wang, Black phosphorus nanosheets-enabled DNA hydrogel integrating 3D-printed scaffold for promoting vascularized bone regeneration, Bioact. Mater. 21 (2023) 97–109.
[12] R.C. Gresham, C.S. Bahney, J.K. Leach, Growth factor delivery using extracellular matrix-mimicking substrates for musculoskeletal tissue engineering and repair, Bioact. Mater. 6 (7) (2021) 1945–1956.
[13] Z. Lv, T. Hu, Y. Bian, G. Wang, Z. Wu, H. Li, X. Liu, S. Yang, C. Tan, R. Liang, A MgFe-ldh nanosheet-incorporated smart thermo-responsive hydrogel with controllable growth factor releasing capability for bone regeneration, Adv. Mater. 35 (5) (2023), 2206545.
[14] Y. Wei, G. Zhu, Z. Zhao, C. Yin, Q. Zhao, H. Xu, J. Wang, J. Zhang, X. Zhang, Y. Zhang, Individualized plasticity autograft mimic with efficient bioactivity inducing osteogenesis, Int. J. Oral Sci. 13 (1) (2021) 14.
[15] N.Z. Laird, T.M. Acri, K. Tingle, A.K. Salem, Gene-and RNAi-activated scaffolds for bone tissue engineering: current progress and future directions, Adv. Drug Deliv. Rev. 174 (2021) 613–627.
[16] K.W.-H. Lo, B.D. Ulery, K.M. Ashe, C.T. Laurencin, Studies of bone morphogenetic protein-based surgical repair, Adv. Drug Deliv. Rev. 64 (12) (2012) 1277–1291.
[17] L. Wu, Y. Xu, K. Xi, Y. Gu, J. Tang, T. Xin, H. Yang, L. Wang, W. Cui, L. Chen, Regulation of macrophage subtype via injectable micro/nano-structured porous microsphere for reprogramming osteoimmune microenvironment, Chem. Eng. J. 439 (2022), 135692.
[18] G. Walters, I. Pountos, P.V. Giannoudis, The cytokines and micro-environment of fracture haematoma: current evidence, J. Tissue Eng. Regener. Med. 12 (3) (2018) e1662–e1677.
[19] Q. Chen, J. Li, F. Han, Q. Meng, H. Wang, Q. Wei, Z. Li, F. Li, E. Xie, X. Qin, A multifunctional composite hydrogel that rescues the ROS microenvironment and guides the immune response for repair of osteoporotic bone defects, Adv. Funct. Mater. 32 (27) (2022), 2201067.
[20] J. Li, F. Han, J. Ma, H. Wang, J. Pan, G. Yang, H. Zhao, J. Zhao, J. Liu, Z. Liu, Targeting endogenous hydrogen peroxide at bone defects promotes bone repair, Adv. Funct. Mater. 32 (10) (2022), 2111208.
[21] P. Graney, S. Ben-Shaul, S. Landau, A. Bajpai, B. Singh, J. Eager, A. Cohen, S. Levenberg, K. Spiller, Macrophages of diverse phenotypes drive vascularization of engineered tissues, Sci. Adv. 6 (18) (2020), eaay6391.
[22] C. Han, M. Guo, J. Bai, L. Zhao, L. Wang, W. Song, P. Zhang, Quercetin-loaded nanocomposite microspheres for chronologically promoting bone repair via synergistic immunoregulation and osteogenesis, Mater. Des. 222 (2022), 111045.
[23] J. Kushioka, S.K.-H. Chow, M. Toya, M. Tsubosaka, H. Shen, Q. Gao, X. Li, N. Zhang, S.B. Goodman, Bone regeneration in inflammation with aging and cell-based immunomodulatory therapy, Inflamm. Regen. 43 (1) (2023) 1–13.
[24] O.R. Mahon, D.C. Browe, T. Gonzalez-Fernandez, P. Pitacco, I.T. Whelan, S. Von Euw, C. Hobbs, V. Nicolosi, K.T. Cunningham, K.H. Mills, Nano-particle mediated M2 macrophage polarization enhances bone formation and MSC osteogenesis in an IL-10 dependent manner, Biomaterials 239 (2020), 119833.
[25] C. Han, Y. Sheng, J. Wang, X. Zhou, W. Li, C. Zhang, L. Guo, Y. Yang, NOX4 promotes mucosal barrier injury in inflammatory bowel disease by mediating macrophages M1 polarization through ROS, Int. Immunopharm. 104 (2022), 108361.
[26] M. Sandor, D. Enscore, P. Weston, E. Mathiowitz, Effect of protein molecular weight on release from micron-sized PLGA microspheres, J. Contr. Release 76 (3) (2001) 297–311.
[27] J. Liu, Y. Xu, Y. Wang, H. Ren, Z. Meng, K. Liu, Z. Liu, H. Huang, X. Li, Effect of inner pH on peptide acylation within PLGA microspheres, Eur. J. Pharmaceut. Sci. 134 (2019) 69–80.
[28] G. Zhu, S.R. Mallery, S.P. Schwendeman, Stabilization of proteins encapsulated in injectable poly (lactide-co-glycolide), Nat. Biotechnol. 18 (1) (2000) 52–57.
[29] Z. Meng, Y. Zhang, J. She, X. Zhou, J. Xu, X. Han, C. Wang, M. Zhu, Z. Liu, Ultrasound-mediated remotely controlled nanovaccine delivery for tumor vaccination and individualized cancer immunotherapy, Nano Lett. 21 (3) (2021) 1228–1237.
[30] Z. Liu, S. Zhang, H. Lin, M. Zhao, H. Yao, L. Zhang, W. Peng, Y. Chen, Theranostic 2D ultrathin MnO2 nanosheets with fast responsibility to endogenous tumor microenvironment and exogenous NIR irradiation, Biomaterials 155 (2018) 54–63.
[31] Y. Li, Q. Pan, J. Xu, X. He, H.A. Li, D.A. Oldridge, G. Li, L. Qin, Overview of methods for enhancing bone regeneration in distraction osteogenesis: potential roles of biometals, J. Orthop. Translat. 27 (2021) 110–118.
[32] Z. Yuan, Z. Wan, P. Wei, X. Lu, J. Mao, Q. Cai, X. Zhang, X. Yang, Dual-controlled release of icariin/Mg2+ from biodegradable microspheres and their synergistic upregulation effect on bone regeneration, Adv. Healthcare Mater. 9 (11) (2020), 2000211.
[33] G. Yang, L. Xu, Y. Chao, J. Xu, X. Sun, Y. Wu, R. Peng, Z. Liu, Hollow MnO2 as a tumor-microenvironment-responsive biodegradable nano-platform for combination therapy favoring antitumor immune responses, Nat. Commun. 8 (1) (2017) 902.
[34] Z.-h. Zhou, S.-y. Liang, T.-c. Zhao, X.-z. Chen, X.-k. Cao, M. Qi, Y.-y. Huang, W.-t. Ju, M. Yang, D.-w. Zhu, Overcoming chemotherapy resistance using pH-sensitive hollow MnO2 nanoshells that target the hypoxic tumor microenvironment of metastasized oral squamous cell carcinoma, J. Nanobiotechnol. 19 (1) (2021) 157.
[35] X. Xu, J. Duan, Y. Liu, Y. Kuang, J. Duan, T. Liao, Z. Xu, B. Jiang, C. Li, Multi-stimuli responsive hollow MnO2-based drug delivery system for magnetic resonance imaging and combined chemo-chemodynamic cancer therapy, Acta Biomater. 126 (2021) 445–462.
[36] J. Liu, F. Li, X. Li, X. He, Ultrathin MnO2 nanosheets grown on hollow carbon spheres with enhanced capacitive performance, Phys. Lett. 384 (22) (2020), 126539.
[37] Q. Chen, L. Feng, J. Liu, W. Zhu, Z. Dong, Y. Wu, Z. Liu, Intelligent albumin–MnO2 nanoparticles as pH-/H2O2-responsive dissociable nanocarriers to modulate tumor hypoxia for effective combination therapy, Adv. Mater. 28 (33) (2016) 7129–7136.
[38] H. Aro, E. Eerola, A. Aho, J. Niinikoski, Tissue oxygen tension in externally stabilized tibial fractures in rabbits during normal healing and infection, J. Surg. Res. 37 (3) (1984) 202–207.
[39] B.R. Barrioni, E. Norris, S. Li, P. Naruphontjirakul, J.R. Jones, M.d.M. Pereira, Osteogenic potential of sol–gel bioactive glasses containing manganese, J. Mater. Sci. Mater. Med. 30 (2019) 1–15.
[40] Y.-J. Bae, M.-H. Kim, Manganese supplementation improves mineral density of the spine and femur and serum osteocalcin in rats, Biol. Trace Elem. Res. 124 (2008) 28–34.
[41] H.Y. Kim, S.Y. Kim, H.-Y. Lee, J.H. Lee, G.-J. Rho, H.-J. Lee, H.-C. Lee, J.-H. Byun, S.H. Oh, Oxygen-releasing microparticles for cell survival and differentiation ability under hypoxia for effective bone regeneration, Biomacromolecules 20 (2) (2019) 1087–1097.